Nanostructures of $Mg_{0.65}Ti_{0.35}D_x$ studied with x-ray diffraction, neutron diffraction, and magic-angle-spinning ^2H NMR spectroscopy

S. Srinivasan,[1] P. C. M. M. Magusin,[1,*] W. P. Kalisvaart,[2] P. H. L. Notten,[1,3] F. Cuevas,[4] M. Latroche,[4] and R. A. van Santen[1]

[1]*Eindhoven University of Technology, P.O. Box 513, 5600 MB Eindhoven, The Netherlands*

[2]*University of Alberta, 9107 116 Street, Edmonton, Alberta, Canada T6G 2V4*

[3]*Philips Research Laboratories, High Tech Campus 4, 5656 AE Eindhoven, The Netherlands*

[4]*Institut de Chimie et des Materiaux de Paris-Est, UMR 7182, CNRS, 2-8, Rue Henri Dunant, 94320 Thiais, France*

(Received 2 August 2009; revised manuscript received 30 November 2009; published 10 February 2010)

Magnesium transition-metal alloys have a high hydrogen-storage capacity and show improved hydrogen-uptake and -release kinetics compared to magnesium alone. In the present study we have investigated the structure of bulk magnesium-titanium deuteride $Mg_{0.65}Ti_{0.35}D_x$ prepared via mechanical alloying and gas-phase deuterium absorption by combined use of x-ray diffraction (XRD), neutron diffraction, and magic-angle-spinning ^2H nuclear magnetic resonance (NMR). The initial ball-milled alloy has two XRD-distinct Mg and Ti fcc phases. Even after prolonged exposure to deuterium gas at 75 bar and 175 °C the materials with and without palladium catalyst are only partly deuterated. Deuterium loading causes the formation of, on the one hand, bct (rutile) MgD_2 nanodomains with interdispersed TiD_y layers and, on the other hand, a separate fcc (fluorite) TiD_z phase. The TiD_y phase is XRD invisible, but shows clearly up at a ^2H NMR shift of −43 ppm between the shift of MgD_2 (3 ppm) and the Knight shift of the TiD_z phase (−143 ppm). Exchange NMR indicates complete deuterium exchange at 25 °C between the MgD_2 and TiD_y phase within 1 s, as consistent with intimate contacts between these phases. Combined analysis of the XRD and NMR peak areas suggests that the deuterium concentrations y and z in the TiD_y and TiD_z domains are about 1.5 and 2.0, respectively. Comparing the intrinsic cell parameters of rutile MgH_2 and fluorite TiH_2, we propose that stabilization of the mixed nanocomposite may arise from a coherent coupling between the crystal structures of the rutile MgD_2 nanodomains and the thin layers of fcc TiD_y.

DOI: 10.1103/PhysRevB.81.054107 PACS number(s): 61.66.Dk, 84.60.−h, 66.30.Fq, 76.60.−k

I. INTRODUCTION

The increasing demand for energy puts the conventional fossil fuel sources under stress as these are already running out. An attractive alternative energy carrier would be hydrogen, if it can be efficiently stored. This can be achieved by means of pressurized gas or liquefied hydrogen. However, high pressure (typically 70 MPa) or low temperature (21 K) are necessary to reach practical capacities. Alternative options at lower pressure and higher temperature are physical hydrogen storage in porous materials[1,2] or chemical hydrogen storage in the form of hydride compounds, such as reversible metal hydrides.[3] Metal-based hydrogen storage materials have the advantage of being operable under closer to ambient conditions when compared to other types of storage. The typical usage would be for stationary hydrogen storage or for electrode materials in rechargeable batteries for portable devices such as cell phones and cameras. Since hydrogen is absorbed in metal hydrides as atoms, rather than molecules, these hydrides typically have a volumetric hydrogen density similar to or higher than liquid hydrogen (71 kg m^{-3} at 20 K).[4] Magnesium hydride, for instance, can theoretically store 110 kg m^{-3}, and because magnesium is a light metal, it also has a high *gravimetric* storage capacity of 7.6 wt. % hydrogen. However, MgH_2 suffers from slow sorption kinetics. Notten and co-workers[5–7] have recently found that the kinetics can be improved by alloying magnesium with scandium. A Sc fraction >20 at. % transition metal causes a change from the rutile structure of MgH_2 to a fluorite structure of transition-metal hydrides and thereby enhances the mobility of the hydrogen.[8] As revealed by NMR relaxometry[9] hydrogen mobility is significantly faster in $Mg_{0.65}Sc_{0.35}H_{2.2}$ than in MgH_2 and ScH_2. Since scandium is a precious metal, an economically more feasible option is to use its less expensive neighbor in the periodic table of elements, titanium, which has similar electrochemical properties in Mg-based thin films as scandium.[10]

Magnesium and titanium are thermodynamically immiscible,[11] but alloys can be produced, e.g., in the form of thin films by e-beam deposition,[10] physical vapor deposition[12] and magnetron cosputtering,[13] or as bulk powders by mechanical mixing.[14–19] The boiling point of Mg is less than the melting point of Ti which rules out melt mixing techniques. The crystal structure of pure Mg and Ti is hexagonal, but ball milling of mixed Mg and Ti powders with micron-sized particles yields a material with two face-centered cubic (fcc) crystal phases.[18] This is promising for its properties as a hydrogen storage material, because an fcc Mg-Ti lattice with hydrogen at the tetrahedral (T) interstitial sites would form the favorable fluorite ternary compound. Indeed, thin *films* of magnesium-titanium hydride have a coherent fcc crystalline structure with a composition-dependent lattice constant,[20–22] and show strongly enhanced kinetics of hydrogen uptake and release compared to thin magnesium hydride films without titanium.[23] In addition, compressing the *hydrides* MgH_2 and $TiH_{1.9}$ at high temperature (600 °C) and pressure (8 GPa) yields single-phase Mg_7TiH with an fcc unit cell (4.77 Å) as the basic structure building block of a superstructure with nonrandom ordering of Mg and Ti atoms over the metal positions.[24,25]

X-ray diffraction (XRD) is commonly employed to characterize the crystal structure of metal hydrides and gives information about the lattice positions of the metal atoms. Due to the high scattering of the metal atoms hydrogen and deuterium are not observable with XRD. This is especially the case in conducting materials, in which the electron of hydrogen or deuterium atoms is delocalized. These light atoms are visible with neutron diffraction (ND), because neutrons interact with the atomic nuclei, rather than the electrons. Both XRD and ND require structural coherence in sufficiently large crystalline domains or particles. These techniques cannot detect amorphous domains or ordered domains with too short coherence lengths. In contrast, nuclear magnetic resonance (NMR) spectroscopy does not require crystallinity. Magic-angle-spinning (MAS) ^{1,2}H NMR spectroscopy gives direct information about the local chemical environment of hydrogen or deuterium in metal hydrides or deuterides. Although the NMR frequency of ^{1}H nuclei is higher than that of ^{2}H nuclei at a given magnetic field, the chemical resolution in ^{2}H NMR spectra of metal deuterides tends to be actually higher than in ^{1}H NMR spectra of the corresponding metal hydrides[9,26,27] This is because the dipolar coupling between ^{1}H nuclei is also stronger than between ^{2}H nuclei at the same internuclear distance. As a consequence, MAS ^{1}H NMR lines tend to be broadened by higher-order multispin effects not completely averaged by the sample rotation. For magnesium-scandium deuteride we were recently able to distinguish quantitatively between deuterium atoms with pure magnesium coordination and those with at least one scandium neighbor, and establish the rate at which deuterium exchanges between these two environments. This yielded insight into the nonrandom ordering of Sc and Mg over the metal positions in the lattice at a length scale below the coherence length required for XRD and ND.

In the present study we combine x-ray powder diffraction, neutron powder diffraction, and MAS ^{2}H NMR spectroscopy to characterize bulk magnesium-titanium deuteride prepared via mechanical alloying of Mg and Ti and subsequent deuterium absorption at 175 °C.

II. EXPERIMENTAL SECTION

The two ball-milled Mg-Ti alloys (with and without Pd catalyst) in this paper were synthesized by mechanical mixing of Mg and Ti powders (particle size <50 μm) in a Spex 8000 ball mill at 1750 rpm. The powders were loaded in a 55 ml vial with tungsten-carbide lining together with 12 stainless steel balls of 10 mm diameter. Ball-to-powder weight ratio was 16 to 1. 1.5 wt. % of stearic acid was added as a process-control agent at the start of the milling process to reduce cold welding of the powder. After 5 h of milling, the alloy (without Pd catalyst) was loaded into a Parr high-pressure vessel and exposed to 75 bar deuterium gas and heated to 175 °C for ~24 h. The other MgTi alloy was activated by milling for 90 min with 2 at. % of Pd as hydrogen-absorption catalyst prior to the ND experiment. A total amount of 4.85 g of the obtained $Mg_{0.65}Ti_{0.35}Pd_{0.02}$ was introduced in a stainless steel cylindrical container connected to a manometric device allowing *in situ* loading and unloading of the sample with deuterium gas (Sievert's method) inside the ND measuring device. The sample holder was first evacuated under secondary vacuum (10^{-4} mbar) and then introduced in a furnace at the center of the diffractometer. Two reference samples were prepared by ball milling. The TiD_2 was obtained by ball milling the Ti powder for 1 h and subsequent deuterium loading under high pressure and temperature (450 °C). MgD_2 was prepared in a similar way with two ball-milling steps followed by deuterium loading at 75 bar and 300 °C.

Ex situ x-ray powder diffraction of the material before and after deuterium loading was measured on a PANalytical X'Pert-Pro MPD diffractometer by use of an X'Celerator detector or on a Rigaku D/MAX-B. Data were collected over a 2θ angular range of $10°-100°$ using Cu $K\alpha$ radiation at 40 kV and 40 mA. The materials were measured at room temperature with normal exposure to air.

In situ neutron powder diffraction patterns have been recorded for different temperature and hydrogen-pressure ranges with the position sensitive detector (PSD) of the D1B instrument at the Institut Laue Langevin in Grenoble. The wavelength was set to 1.287 Å and the patterns were recorded every 5 min for absorption and every 10 min for desorption in the range $18°-98°$ by the 400 cells of the PSD (step=0.2° in 2θ). The diffraction patterns were sequentially refined using the program FULLPROF.[28]

Ex situ ^{2}H NMR spectra of the material after deuterium loading were recorded on a Bruker DMX500 spectrometer operating at a ^{2}H NMR frequency of 76.7 MHz. MAS was applied to eliminate the first-order line broadening effect of the quadrupolar interaction. The typical sample-rotation rates were between 8 and 24 kHz. The NMR sample holder was packed at room temperature in normal air, closed with a tight cap and rotated in a flow of dry nitrogen inside the spectrometer. Two-dimensional exchange spectroscopy (2D Exsy) was carried out by use of the standard pulse sequence consisting of three 90° pulses of 5 μs each.[29] The time interval between the first two pulses (evolution time t_1) was systematically incremented in the course of the experiment, while the time interval between the second and third pulses (mixing time t_{mix}) was fixed to either 0.01, 1, or 5 s. For 2D Exsy, the microcrystalline $Mg_{0.65}Ti_{0.35}D_x$ powder was packed into 4 mm MAS sample holders and rotated at a rate of 14 kHz. One-dimensional Exsy (1D Exsy) was measured by selectively perturbing the polarization of the deuterium nuclei in the MgD_2 phase resonating at 3 ppm using a rotor-synchronized DANTE pulse train[30] of six soft pulses of 1 μs at a reduced rf power level corresponding to a ^{2}H mutation frequency of 12.5 kHz, and monitoring the polarization a variable time interval (mixing t_{mix}) later by means of a nonselective 90° read pulse of 5 μs. The one-dimensional exchange spectra were recorded at varied mixing times between 0.01 and 1 s and varied temperatures between −75 and 25 °C to monitor the possible deuterium exchange from the MgD_2 phase to the other two phases. For 1D Exsy the sample was packed into a 2.5 mm MAS rotor and spun at a rate of 20 kHz. The exchange curves were always compared with the T_1 relaxation observed after nonselective perturbation resulting from replacing the DANTE pulse train by a single nonselective 90° pulse. Because of its high specific

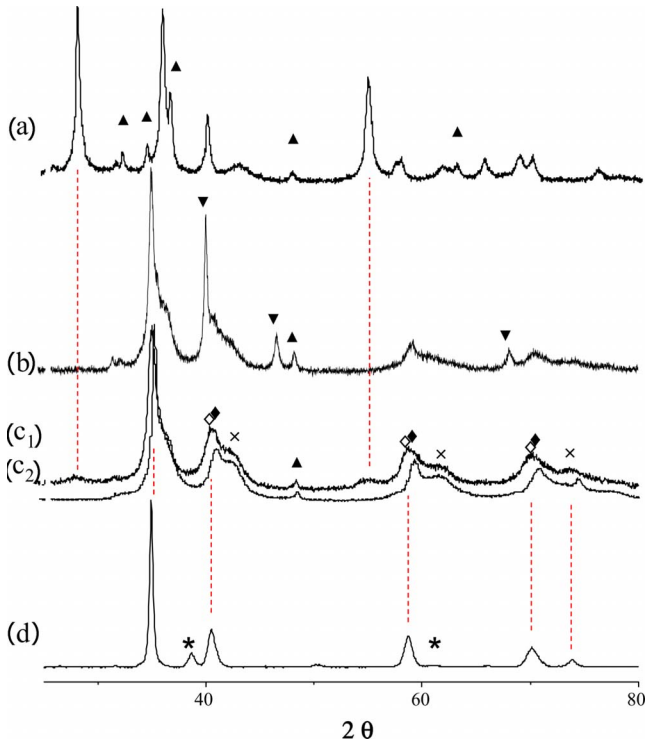

FIG. 1. (Color online) XRD pattern of (a) MgD_2, (b) $Mg_{0.65}Ti_{0.35}Pd_{0.02}$, ($c_1$) $Mg_{0.65}Ti_{0.35}D_x$, (c_2) $Mg_{0.65}Ti_{0.35}$, and (d) TiD_2. ♦ fcc Mg-rich (4.42 Å), × fcc Ti-rich (4.26 Å), ◇ fcc TiD_2,* hcp Ti, ▲ hcp Mg, and ▼ fcc Pd (3.89 Å).

weight, TiD_2 was mixed with alumina to obtain stable sample rotation. The ternary system $Mg_{0.65}Ti_{0.35}D_x$ was not diluted with alumina because it was spinning without any problem at high MAS speeds. MAS ^{2}H NMR sideband patterns were analyzed in combination with static ^{2}H NMR line shapes using the spectrum fit program DMFIT (2008 version).[31]

III. RESULTS

A. XRD characterization

Figure 1 shows the XRD patterns of the ball-milled magnesium-titanium alloys with and without Pd catalyst (b and c_2), and the deuterium-loaded ball-milled alloy without Pd (c_1). For comparison, the patterns of (a) MgD_2 and (d) TiD_2 are shown, as well. All patterns were deconvoluted in terms of Gaussian-Lorentzian line shapes and the extracted peak positions and widths are given as supplementary data.[32] The Pd-containing alloy was the sample investigated with neutron diffraction (vide infra) and the deuterium-loaded material without Pd was investigated with ^{2}H NMR (see below). The MgD_2 has a rutile structure with lattice constants a=4.516(8) Å and c=3.011(5) Å. There are also reflections from a small amount of hcp Mg. The x-ray pattern of TiD_2 shows the main fcc hydride phase with cell parameter 4.444(2) Å (consistent with Ref. 33), as well as a minor hcp Ti phase. The XRD reflections of the magnesium-titanium alloys with and without Pd are broad, which is indicative for small crystalline-domain sizes. Both materials have two fcc phases, the smaller one of which (cell parameters 4.28(2) Å in $Mg_{0.65}Ti_{0.35}$ and 4.33 Å in $Mg_{0.65}Ti_{0.35}Pd_{0.02}$) is assigned to a Ti-rich phase on the basis of published lattice constants of fcc Ti metal (4.34 Å) (Ref. 34) and $Ti_{0.94}Mg_{0.06}$ alloy (4.26 Å).[35] It has been reported before that ball milling causes the pure titanium metal to undergo a structure transition from hcp to fcc, as well.[34] The fcc phase with the larger constant, 4.42 Å, both for alloys with and without Pd, is assigned to a Mg-rich phase. The (111) reflection (around 2θ=35°) of this phase is narrow compared to the other reflections for both alloys, indicating longer coherence length (25 nm) in this direction than in other directions (~3–9 nm).[32] The molar volume of this phase, 13.0 $cm^3\ mol^{-1}$, lies between the molar volumes 14.0 and 10.6 $cm^3\ mol^{-1}$ of pure Mg and Ti in the hcp phase, respectively. Such a molar volume can be interpreted according to Vegard's law[36] in terms of a phase composition $Mg_{0.71}Ti_{0.29}$, which is close to the overall composition $Mg_{0.65}Ti_{0.35}$. However, given the fact that a significant Ti fraction resides in the Ti-rich phase, the relative Mg content in the Mg-rich phase is probably higher. The alloy with Pd coating (added at the end of the ball milling) also shows the reflections from a separate fcc Pd phase with lattice constant 3.89 Å.

Upon prolonged exposure to deuterium at 175 °C and 75 bar, the XRD reflections of $Mg_{0.65}Ti_{0.35}$ alloy have become weaker, but stay at approximately the same angles. At close inspection, it turns out that the XRD peaks of the originally 4.42 Å fcc phase show slight broadening toward smaller reflection angles. At first thought, we have considered a small lattice expansion of the Mg-rich fcc phase upon deuterium uptake. Because of the above-mentioned different molar volumes of Mg and Ti, however, one would expect such Mg-rich deuteride fcc phase to have a substantially larger cell parameter than fcc TiD_2 (4.44 Å), probably similar to the computed value for fcc MgH_2 (4.79 Å),[37] and the experimentally found value of $Mg_{0.65}Sc_{0.35}D_{2.2}$ (4.81 Å).[8] However, such fcc phase is not observed (Fig. 1). Therefore, as an alternative explanation, the asymmetric broadening toward lower reflection angles could also indicate the formation of fcc $TiD_{z\sim2}$ upon deuterium absorption. In addition to this asymmetric broadening, wide reflections at the positions of rutile MgD_2 become also visible after deuterium loading. Indeed, the XRD pattern of $Mg_{0.65}Ti_{0.35}D_x$ is quite well described as a linear combination of the patterns of the initial alloy $Mg_{0.65}Ti_{0.35}$, on the one hand, and the pure deuterides MgD_2 and TiD_2, on the other [Fig. 2(a)]. Deuterium loading of the magnesium-titanium alloy thus appears to cause the material to segregate into bct MgD_2 and fcc $TiD_{z\sim2}$. Magnesium hydride always occurs as the stoichiometric MgH_2. At lower overall hydrogen concentration, the hydride separates into a MgH_2 phase and almost $MgH_{\sim0.001}$.[38] Titanium hydride exists in varying nonstoichiometric states. These TiH_z compounds have an fcc crystal structure with a lattice constant slightly depending on the hydrogen concentration z (Table I). Even after prolonged exposure of the alloy $Mg_{0.65}Ti_{0.35}$ to deuterium, part of the original Mg-rich and Ti-rich phases has not become deuterated. As shown later in this paper, ND and NMR analyses qualitatively support this interpretation. The implicit suggestion from the XRD analysis that the Mg-rich and Ti-rich phases are equally converted,

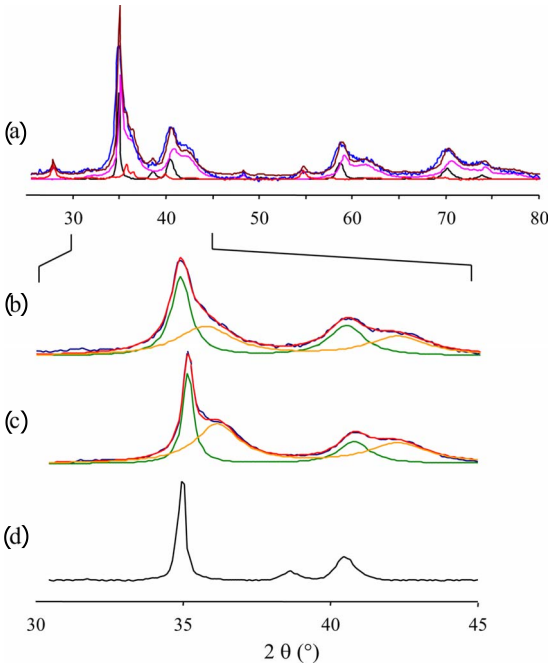

FIG. 2. (Color online) Analysis of the XRD pattern of $Mg_{0.65}Ti_{0.35}D_{0.65}$. (a) Linear regression in terms of the observed patterns of $Mg_{0.65}Ti_{0.35}$, TiD_2, and MgD_2 (Fig. 1); [(b) and (c)] Coupled deconvolution of the inhomogeneous (111) and (200) reflections of (b) $Mg_{0.65}Ti_{0.35}D_x$ and (c) $Mg_{0.65}Ti_{0.35}$ with the overall peak-area ratio $A_{111}:A_{200}=1.4$ as a fit restriction for the individual components, as well. (d) observed pattern of TiD_2 for comparison.

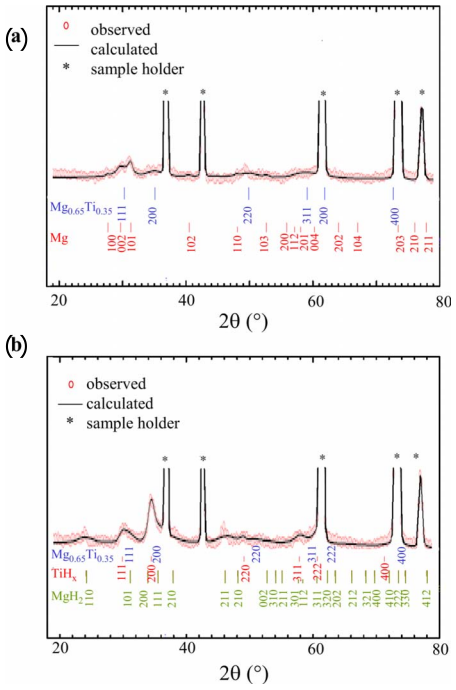

FIG. 3. (Color online) Refined neutron-diffraction pattern [measured (open circles) and calculated (solid line)] for the alloy $Mg_{0.65}Ti_{0.35}Pd_{0.02}$ (a) before and (b) after deuterium absorption. Vertical bars correspond to diffraction line positions for each phase. Stars indicate the sharp lines arising from the stainless steel container.

however, is probably an artifact of the linear regression model, which treats the XRD pattern of the alloy as one of the invariant components. Furthermore, the rutile reflections of the MgD_2 phase formed during deuterium uptake are obviously much broader than those of MgD_2, and the (111) reflection of the $TiD_{z\sim2}$ phase in the ternary system is also broader than that of the TiD_2 reference compound. Broad reflections are typical of crystalline nanostructures with a small coherence length.

B. ND characterization

Before starting the *in situ* deuterium-loading ND experiment, the $Mg_{0.65}Ti_{0.35}Pd_{0.02}$ sample was measured in the beam (at time $t=0$). Figure 3(a) shows the refinement of this first pattern. The five sharp lines marked with stars in the figure belong to the stainless steel sample holder. Beside these lines, tiny lines belonging to the sample were observed. They have been identified as an averaged main phase ($Mg_{0.65}Ti_{0.35}$) adopting an fcc structure with cell parameter $a=4.40(2)$ and pure hcp magnesium [$a=3.22(1)$ and $c=5.21(4)$ Å]. As a consequence of the limited resolution of the instrument, it was not possible to distinguish in the refinement between the 4.28 and 4.42 Å fcc phases recognized in the XRD patterns. Although Mg lines look stronger than those of the fcc phase, the relative amount of Mg is low (~3 wt. %). This results from the fact that hcp Mg has a positive Fermi length ($b_{Mg}=0.5375$), whereas the fcc phase is made by alloying Mg and Ti with positive and negative Fermi length ($b_{Mg}=0.5375$ and $b_{Ti}=-0.3438$) leading to weaker intensities for this latter phase.

Deuterium gas was introduced into the sample holder and both diffraction pattern and pressure evolutions were followed. For the first step, 24.8 bar of D_2 was introduced into the device, but only little absorption, 0.014 deuterium atom per metal atom (D/M), was observed. After 20 min, a second amount of gas ($P=24$ bar) was added to the system. After 629 min, the total absorbed amount was estimated to be 0.163 D/M but the pressure drop remained very slow. To speed up the absorption process, the temperature of the sample holder was gradually increased from 14 to 175 °C in steps of ~50 °C. A significant improvement in the kinetics was then observed. The pressure decreased rapidly and the deuterium uptake reached 0.94 D/M after 853 min. A third

TABLE I. Cell parameters for fluorite and rutile MgH_2, and fluorite ScH_2 and TiH_z at varying hydrogen content z. The value for fluorite MgH_2 is a theoretical prediction based on two consistent DFT studies (Refs. 37 and 55). Other values have been experimentally determined.

	Fluorite (Å)	Rutile (Å)
MgH_2	$a=4.79$	$a=4.52$
		$c=3.01$
ScH_2	$a=4.78$	
TiH_2	$a=4.44$	
$TiH_{1.8}$	$a=4.44$	
$TiH_{1.23}$	$a=4.39$	

amount of deuterium was again added to the system (P=24.56 bar) and a small extra uptake was obtained (1.01 D/M). The sample was then cooled down to room temperature and the final deuterium content at room temperature reached 1.03 D/M.

During the reported absorption process, a series of neutron diffractograms were recorded as a function of time.[32] After 480 min, new lines attributed to bct (rutile) MgD_2 and fcc TiD_z are appearing. These lines become stronger as a function of deuterium loading and are observed till the end of the absorption process. A typical refined pattern taken after 880 min of absorption is shown in Fig. 3(b). This pattern shows the coexistence of at least three phases: the averaged fcc $Mg_{0.65}Ti_{0.35}$ phase with lattice constant a=4.34(4) and two deuteride phases, bct MgD_2 [a=4.56(3) Å and c =2.96(3) Å], and fcc TiD_z [a=4.478(5) Å] in the weight ratio 73(27)%, 8(2)%, and 19(8)%, respectively. The large error (±27%) for the main phase is related to its poor scattering factor and strong overlap with neighboring diffraction lines from other phases. The TiD_z lattice constant determined with ND is 1% larger than the value 4.44 Å for the TiD_z phase estimated from XRD. However, the XRD value could only be accurately determined for *pure* TiD_2. Estimation of the cell parameter for this phase in $Mg_{0.65}Ti_{0.35}D_x$ from the XRD pattern is complicated by the overlap with the reflections of the nondeuterated Mg-rich phase (Figs. 1 and 2). The advantage of the poor ND visibility of the nondeuterated main phase is a better resolution of the ND signals of the TiD_z phase. The diffraction patterns have been refined sequentially. From this data analysis, the amount and volume of each phase can be extracted and are given in Fig. 4(a), respectively, as a function of loading time. Finally, the two possible available sites (octahedron and tetrahedron) for deuterium in the TiD_z phase were also tentatively refined. This shows that only the T site is significantly occupied with about 1.2 ± 0.25 D/M, whereas the octahedral (O) site is nearly empty. From the absorption study, it can be concluded that upon deuteration the averaged fcc phase partially transforms into MgD_2 and TiD_z with $z \sim 1.2$. The latter deuterium concentration, z, is best regarded as an underestimate, because the large cell parameter 4.478 Å indicates a higher deuterium content (Table I). The transformation of the alloy into MgD_2 and TiD_z is enhanced by raising the temperature to 175 °C. However, despite this thermal improvement, the reaction was not complete after 16 h.

After absorption, the sample was thermally discharged using temperature programmed desorption. The heating rate was set to 1 K/min from room temperature up to 730 K (457 °C). To improve the counting statistics, each pattern was measured for 10 min. A sharp pressure increase is observed above 180 °C up to 300 °C [Fig. 4(b)], which is attributed to deuterium desorption from the sample. Above 275 °C the MgD_2 reflections disappear and new lines attributed to pure Mg become visible. The diffraction patterns have been refined sequentially for the whole thermal-desorption experiment. From this analysis the fractions of the different phases have been extracted at as a function of time. The amount of the averaged main fcc phase remains nearly constant during temperature programed desorption (TPD) and does not seem affected by the thermal treatment. The

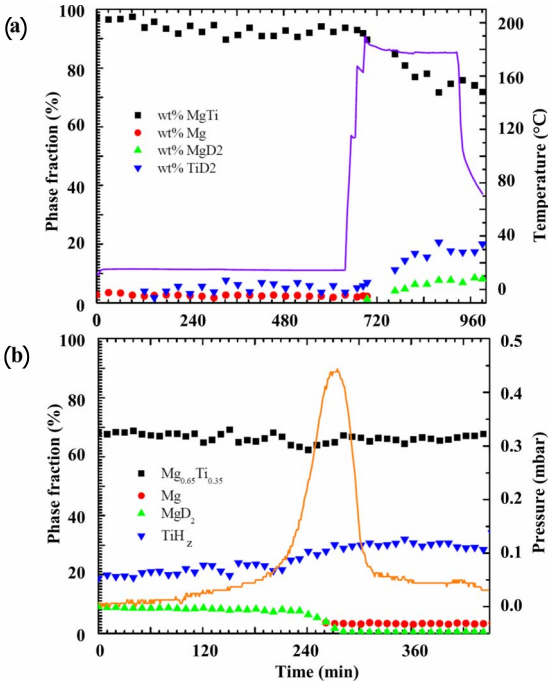

FIG. 4. (Color online) Phase fractions during (a) absorption at 25 °C with a temperature jump to 175 °C after 630 min and (b) temperature-programmed desorption from 40 °C at t=0 to 460 °C at t=420 min (1 K min^{-1}). In the absorption experiment the Mg-Ti fraction stays constant until the temperature is raised to 175 °C. Most of the hydrogen desorption takes places between 180 and 300 °C.

MgD_2 phase desorbs at 280 °C giving rise to the increase in the pressure signal and to the formation of pure Mg. This desorption temperature is in good agreement with the value expected for pure MgD_2. Surprisingly the TiD_2 phase seems to increase. However, this may well be caused by the fact that an increasing fraction of the material becomes amorphous, so that the neutron diffractogram does not reflect the complete quantitative picture. At the end of the TPD process, only three phases are coexisting.

C. NMR characterization

Figure 5 shows the MAS ^{2}H NMR spectra of TiD_2, $Mg_{0.65}Ti_{0.35}D_x$, and MgD_2, as well as $Mg_{0.65}Sc_{0.35}D_{2.2}$, for comparison. At first sight, the spectrum of $Mg_{0.65}Ti_{0.35}D_x$ seems a simple superposition of the MgD_2 and TiD_2 spectra, which confirms a phase separation into MgD_2 and TiD_z as indicated by XRD and ND. Both MgD_2 and the corresponding phase in $Mg_{0.65}Ti_{0.35}D_x$ show a similarly narrow MAS center band at 3 ppm, and similarly intense spinning sidebands caused by the sample rotation [Figs. 5(a) and 5(c)]. The envelope of the sideband pattern reflects the size of the quadrupolar coupling of the deuterium nuclei to local electric field gradients. In combination with the static ^{2}H NMR line shape[32] the extended sideband pattern for MgD_2 [Fig. 5(a)] is well described by a quadrupolar anisotropy ν_Q of 28 kHz and an asymmetry parameter η=0.65. The deuterium atoms at the 4f positions in the rutile MgD_2 structure have a planar

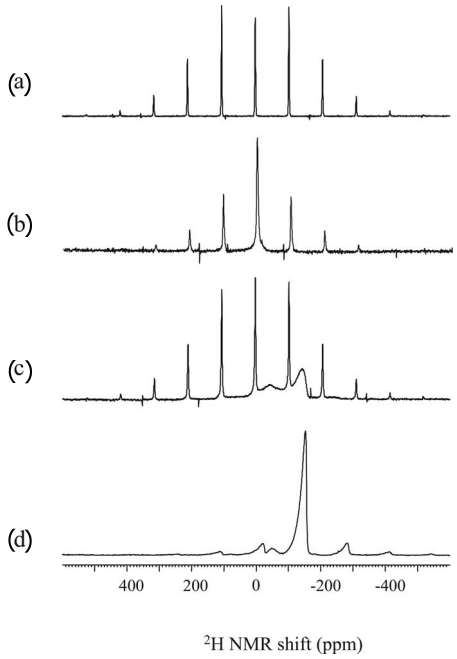

FIG. 5. MAS ^{2}H NMR spectra of (a) MgD_2 at a sample rotation rate of 8 kHz; (b) $Mg_{0.65}Sc_{0.35}D_{2.2}$ at 8 kHz, (c) $Mg_{0.65}Ti_{0.35}D_x$ at 8 kHz, and (d) TiD_2 at 10 kHz.

threefold Mg coordination, resulting in a relatively strong local electric field gradient. In contrast, deuterium atoms in fluorite TiD_2 are located at the tetrahedral interstitial sites, at which the electric field gradient vanishes.[39,40] This is consistent with the relatively weak sidebands observed in Fig. 5(d). The size of the quadrupolar coupling for deuterium in $Mg_{0.65}Sc_{0.35}D_{2.2}$ [Fig. 5(b)] is between that of deuterium in MgD_2 and TiD_2. The sideband pattern is reasonably fitted by various combinations of quadrupolar anisotropy and asymmetry parameters (ν_Q, η) ranging from $\nu_Q=15$ kHz for $\eta=1$ to $\nu_Q=17$ kHz for $\eta=0$, but none of these combinations yields a consistent fit to the static ^{2}H NMR spectrum.[32] The impossibility to consistently describe the sideband pattern and the static NMR line shape by a single component may well reflect a distribution of electric field gradients at the tetrahedral interstitial sites in $Mg_{0.65}Sc_{0.35}D_{2.2}$. This is perhaps associated with the heterogeneous distribution of partial charges in this ternary compound. In addition, motional averaging of the quadrupolar interaction by deuterium mobility could also affect the static line shape and sideband pattern. All in all, the fact that the sideband pattern of the MgD_2 phase in $Mg_{0.65}Ti_{0.35}D_x$ is practically the same as that of pure MgD_2 is consistent with the similar rutile crystal structure also observed with XRD and ND.

The spectrum of TiD_2 and the corresponding phase in $Mg_{0.65}Ti_{0.35}D_x$ contains a signal at −151 and −143 ppm, respectively. Such strongly negative shift values result from the Knight shift typical of conducting materials. The Knight shift depends on the local density of states (LDOS),[41,42] which may vary with position in the crystal structure of a complex metal hydride. For instance, the LDOS in theoretical model structures for Mg-Ti hydrides with random Mg and Ti distribution over the metal positions in the fcc lattice is higher at deuterium sites close to Ti, than Mg atoms.[43] In general, the Knight shift is an anisotropic interaction, i.e., it depends on the orientation of the shift tensor and thus the crystallite with respect to the magnetic field. However, the relatively weak sidebands in the MAS ^{2}H NMR spectrum of TiD_2 [Fig. 5(d)] indicate that the Knight-shift anisotropy for this material is relatively small, as consistent with the cubic crystal structure of TiD_2. Since TiD_2 has a fluorite structure, we assign the signal at −151 for TiD_2 and −143 ppm for $Mg_{0.65}Ti_{0.35}D_x$ to deuterium atoms at the T interstitial sites. MAS ^{2}H NMR of bulk titanium deuteride at varied deuterium content has revealed a stepwise jump from approximately −50 ppm at $D/M<1.5$ to −150 at $D/M>1.7$.[44] The signal at −143 ppm in the ^{2}H NMR spectrum of $Mg_{0.65}Ti_{0.35}D_x$ thus indicates the presence of a TiD_z phase with a rather high deuterium concentration $z>1.7$.

For the ternary system there is an additional signal at −43 ppm with peak area roughly equal to that of the −143-ppm signal. This may be compared with a much smaller signal at −48 ppm in the TiD_2 spectrum. The shift values −43 and −48 ppm suggest deuterium sites in a Ti environment with a lower LDOS. Given its small peak area of a few percent for pure TiD_2, we have considered a possible assignment to a small fraction of deuterium atoms at O sites.[33,45–47] MAS ^{2}H NMR of the second-row transition-metal hydride $YD_{x>2}$, which also has a fcc structure, shows a minor O signal ~27 ppm downfield to the major T signal.[48] For $Mg_{0.65}Ti_{0.35}D_x$, however, no exchange between deuterium sites resonating at −43 and −143 ppm is observed with two-dimensional exchange NMR spectroscopy up to the second time scale (Fig. 6). In short, this technique correlates the chemical shift before and after a selectable time window t_{mix}, during which the deuterium atoms have the opportunity to move to another environment.[49–51] The lack of such correlation between the signals at −43 and −143 ppm in 2D Exsy is inconsistent with the small distance between T and O sites inside the fcc unit cell.

2D Exsy does reveal exchange between deuterium atoms in the MgD_2 phase and the unknown type of sites resonating at −43 ppm (Fig. 6). This suggests an alternative assignment of the −43 ppm signal to small clusters or thin layers of TiD_y dispersed between rutile MgD_2 nanodomains [Fig. 7(b)]. Comparison of the horizontal cross-section at 3 ppm with the overall spectral projection on the horizontal frequency axis shows that at room temperature the exchange between the MgD_2 phase resonating at 3 ppm and the supposed TiD_y clusters resonating at −43 ppm is complete at the second time scale [Fig. 6(b)]. Unlike the isolated TiD_z phase, there is no substantial MgD_2 fraction, which is not close to TiD_y clusters.

The smaller Knight shift, −43 ppm, of deuterium in the TiD_y clusters than in the separate TiD_z phase can be caused by their small size or their lower deuterium content. On the one hand, there have been several reports that the size of the Knight shift decreases upon particle-size reduction.[52,53] In particular, the LDOS appears to be lower at the particle surface, and nanoparticles have a relatively large surface area. However, there is no reason why ball milling would produce a bimodal size distribution, like, in this context, suggested by the two resolved titanium deuteride signals at −43 and

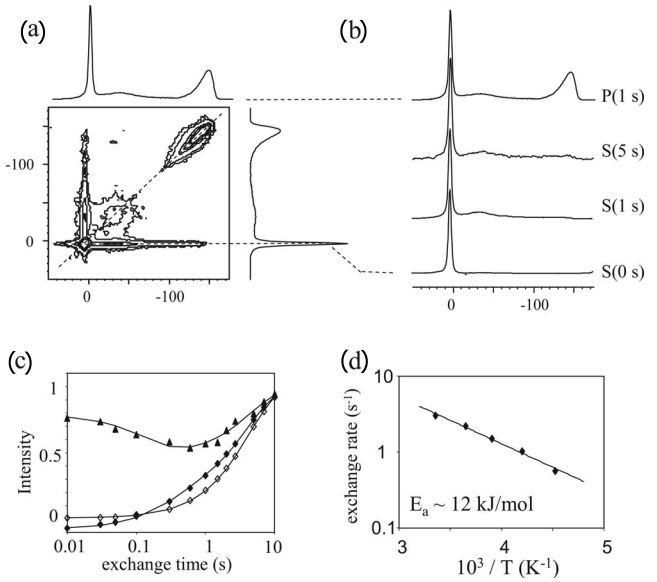

FIG. 6. (a) 2D exchange ^{2}H NMR spectra of $Mg_{0.65}Ti_{0.35}D_x$ at a mixing time of 1 s. Off-diagonal intensity in the 2D spectrum at mixing time $t_{mix}=1$ s indicates deuterium exchange between MgD_2 and TiD_y nanodomains. (b) Projections on the horizontal axis $P(t_{mix})$ and horizontal sections $S(t_{mix})$ crossing the vertical axis at 4 ppm. Comparison of $P(1\ s)$ and $S(1\ s)$ indicates that complete deuteron exchange takes place between MgD_2 and TiD_y nanodomains within 1 s. $S(5\ s)$ shows that hardly any exchange occurs between the TiD_z (macro)phase and MgD_2 or the TiD_y clusters in contact with MgD_2. (c) 1D exchange at 25 °C: transient response of the 3 ppm (♦) and −45 ppm (▲) intensities after selective polarization perturbation of the deuterium spins in the MgD_2 phase resonating at 3 ppm (◇ recovery of the 3 ppm intensity after nonselective perturbation). (d) Temperature dependence of exchange rate extracted from 1D Exsy.

−143 ppm. On the other hand, if the earlier mentioned stepwise loading dependence of the ^{2}H NMR shift observed for bulk TiD_z (Ref. 44) also applies for the titanium deuteride phases in $Mg_{0.65}Ti_{0.35}D_x$, a broad distribution of locally varying deuterium content would effectively produce two ^{2}H NMR resonances. In fact, since smaller metal hydride clusters tend to be thermodynamically less stable, and therefore bind deuterium less strongly,[16] size and deuterium loading are correlated and therefore difficult to disentangle.

2D Exsy yields two-dimensional ^{2}H NMR spectra which can be interpreted in terms of exchange without a prior model. A disadvantage is its generally time-consuming character: recording a single 2D spectrum of $Mg_{0.65}Ti_{0.35}D_{0.65}$ takes about 16 h. We have therefore used 2D Exsy only to confirm our exchange model *qualitatively*. To study the deuterium exchange *quantitatively* as a function of, e.g., time and temperature, we have employed the related 1D Exsy technique.[48,51] Systematic 1D Exsy measurement of the transient response of the deuterium spins in the TiD_y phase at varying mixing times after a selective polarization inversion of the deuterium spins in the MgD_2 phase indicates an exchange time scale of 0.9 s at room temperature [Fig. 6(c)] with only a weak temperature dependence represented by an effective activation energy of 12 kJ mol^{-1} [Fig. 6(d)].

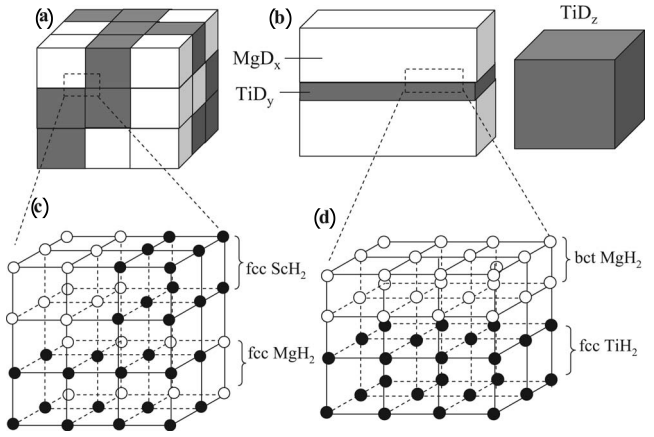

FIG. 7. Mesoscopic picture of for the mixed deuterated phases in (a) $Mg_{0.65}Sc_{0.35}D_{2.2}$ with fcc MgD_2 and ScD_2 nanodomains and (b) $Mg_{0.65}Ti_{0.35}D_x$ with bct MgD_2 nanodomains and fcc layers TiD_y, as well as separate domains TiD_z. [(c) and (d)] Enlarged crystal structure at the phase boundary in the respective materials emphasizing the possible stabilization by coherent coupling of the crystal lattices. (Lattice constants in Table I.)

Roughly comparing deuterium hopping across the boundary between MgD_2 domains and TiD_y clusters with a chemical reaction, like

$$MgD_2 + Ti \leftrightarrow Mg + TiD_2 \tag{1}$$

we find the low barrier of 12 kJ mol^{-1} hard to interpret as a true microscopic parameter. The barrier for such reaction should be bigger than the difference between the formation enthalpies of MgH_2 (−38 kJ/mol H) and TiH_2 (−72 kJ/mol H). Instead, the weak temperature dependence of the deuterium exchange between the MgD_2 nanodomains and the TiD_y clusters could be the signature of a broad range of activation barriers. For a Gaussian distribution $\exp[-(E_a-\langle E_a\rangle)^2/W^2]$ of microscopic barriers E_a with average barrier $\langle E_a\rangle$, distribution width $2W$ and negligible density at $E_a=0$ $(3W<\langle E_a\rangle)$, the behavior in a narrow range around a central temperature T_c would be[54]

$$\left\langle \exp\left(-\frac{E_a}{RT}\right)\right\rangle = \exp\left(-\frac{\langle E_a\rangle}{RT}+\frac{W^2}{(2RT)^2}\right) \approx \exp\left(-\frac{E_{eff}}{RT}\right) \tag{2}$$

with apparent activation energy $E_{eff}=\langle E_a\rangle - W^2/4RT_c$. Here we have used the property $\langle\exp(X)\rangle=\exp[\langle X\rangle+\frac{1}{2}(\langle X^2\rangle-\langle X\rangle^2)]$ of a variable X with Gaussian statistics. At sufficiently low temperature, $2RT_c<W$, E_{eff} can be significantly smaller than the average value $\langle E_a\rangle$ of the true microscopic barriers.

IV. DISCUSSION

According to the combined XRD, ND, and NMR results, the studied material with overall composition $Mg_{0.65}Ti_{0.35}D_x$ has at least five main phases, a Mg-rich and a Ti-rich fcc phase without deuterium, as well as a rutile Mg-rich deuteride and two fcc Ti-rich deuteride phases, respectively, with

and without direct contacts to the rutile Mg-rich deuteride phase. It is interesting to estimate the relative abundances of these phases and see whether a consistent picture can be obtained. Quantitative estimation is not trivial, because the material may have a more complex structure with composition *gradients*, rather than clearcut phase boundaries. Moreover, all of the three applied characterization techniques have their own blind spots. Both XRD and ND require crystallinity over sufficient coherence-length scales. Amorphous domains are undetectable with these techniques. Even for the crystalline domains, deuterium atoms were not detected by XRD in the present study and ND showed low sensitivity resulting from the opposed scattering properties of Mg and Ti in the main phase alloy (but not for MgD_2 and TiD_z). In contrast, deuterium nuclei are directly observed with ^{2}H NMR and no crystallinity is required. However, NMR cannot readily detect the phases without deuterium. In principle, NMR visible isotopes ^{25}Mg and ^{47,49}Ti exist, but their properties are far from NMR friendly. Therefore, a quantitative picture of the material as whole can only be obtained by combining the various techniques.

Let us start with a rough estimate of the composition and relative abundances of the Mg-rich and Ti-rich phases in the alloy *before* hydrogen loading. Deconvolution of the XRD pattern of this material is complicated by the strong overlap between the broad reflections of the Mg- and Ti-rich phases. This tends to yield big correlation errors in the fit parameters. As a kind of regularization we have analyzed the (111) and (200) reflections at ~35° and ~41° in a *coupled* manner under the restriction that the area ratio between the (111) and (200) peaks in each the Mg-rich and Ti-rich pattern is equal to the overall peak-area ratio 1.4, which unambiguously follows from integration. This gives a good fit to the observed XRD pattern [Fig. 2(b)]. From this coupled bicomponent analysis of the (111) and (200) reflections [Fig. 2(a)] a peak-area ratio $R=0.6$ between the Mg-rich and Ti-rich phases can be estimated. To interpret this ratio in terms of the underlying metal-atom fractions in the Mg-rich (ν) and Ti-rich phase ($1-\nu$) with respective compositions $Mg_uTi_{(1-u)}$ and $Mg_wTi_{(1-w)}$, the different x-ray scattering factors of Mg(f_{Mg}) and Ti(f_{Ti}) need to be taken into account. The respective peak areas of the Mg-rich and Ti-rich fcc phases in the XRD pattern are proportional to the square of their effective scattering factors. If the Mg-rich phase $Mg_uTi_{(1-u)}$ has scattering $uf_{Mg}+(1-u)f_{Ti}$ and the Ti-rich phase $Mg_wTi_{(1-w)}$ has scattering factor $wf_{Mg}+(1-w)f_{Ti}$, the relation between the molar and peak-area ratio is implicitly given by

$$\frac{\nu\{uf_{Mg}+(1-u)f_{Ti}\}^2}{(1-\nu)\{wf_{Mg}+(1-w)f_{Ti}\}^2}=R. \tag{3}$$

If all phases are indeed XRD visible (a nontrivial requirement for ball-milled alloys and their hydrides), a second condition follows from the overall Mg fraction 0.65 of the alloy

$$\frac{\nu u+(1-\nu)w}{v(1-u)+(1-v)(1-w)}=\frac{0.65}{0.35}. \tag{4}$$

With $R=0.6$ estimated from the coupled line shape fit, and $f_{Ti}/f_{Mg}=22/12$ from the number of electrons of Ti and Mg atoms, Eqs. (3) and (4) represent two equations with three unknowns. Fortunately, the alloy has also been studied by energy-dispersive x-ray analysis (EDX),[18] which revealed the presence of pure Ti domains with diameters in the order of 0.5 μm, and smaller domains with a Ti content of at least 80 at. %. On this basis, we estimate that the composition w of the Ti-rich phase in the alloy typically ranges between 0 and 0.2. Substitution of these lower and upper bound values for w permits solving Eqs. (3) and (4). For $w=0$, we find $v=0.66$ and $u=0.99$, while for $w=0.2$, $v=0.60$ and $u=0.95$. Thus, the Mg-rich fcc phase with lattice constant 4.42 Å is rather pure, as well. This is quite consistent with the outcome of DFT calculations predicting an fcc Mg structure with lattice constant $a=4.52$ Å, which is only 1.18 kJ mol^{-1} less stable than the usual hcp Mg structure.[55]

Let us return with this information to the deuterated system, and try to find the molar fractions ν_{Ti}, ν_{Mg}, ν_{MgD_2}, ν_{TiD_y}, and ν_{TiD_z} of, respectively, the nondeuterated Ti and Mg phases, the MgD_2 phase and the two deuterated Ti phases TiD_y and TiD_z. Our goal is to determine these fractions and the composition of the TiD_y and TiD_z phases as consistently as possible with the quantitative information from XRD, ND, and NMR.

The basic restriction for this discrete five-phase model is

$$\nu_{Ti}+\nu_{Mg}+\nu_{MgD_2}+\nu_{TiD_y}+\nu_{TiD_z}=1. \tag{5}$$

By assumption, the overall Mg:Ti ratio is conserved during deuterium loading:

$$\frac{\nu_{Ti}+\nu_{TiD_y}+\nu_{TiD_z}}{\nu_{Mg}+\nu_{MgD_2}}=\frac{0.35}{0.65}. \tag{6}$$

Comparing the overall peak area in the ^{2}H NMR spectrum of $Mg_{0.65}Ti_{0.35}D_x$ with known amounts of D_2O and CD_3OD as external reference, we have determined the overall deuterium content $x=0.65$. This value is consistent with the 3.7% weight loss in the thermogravimetric analysis of the NMR sample,[32] but ~1.6 times smaller than the deuterium content of the Pd-free sample studied with ND ($D/M\sim1.03$). The higher loading of the ND sample is probably caused by the Pd catalyst. However, it may also be a consequence of the *in situ* character of the concentration measurement. The deuterium content of the NMR sample was determined *ex situ* by quantitative ^{2}H NMR, and the material may have already lost a particularly unstably bound deuterium fraction before the D/M ratio was determined. The overall deuterium content $x=0.65$ yields the boundary condition:

$$2\nu_{MgD_2}+y\nu_{TiD_y}+z\nu_{TiD_z}=0.65. \tag{7}$$

Deconvolution of the MAS ^{2}H NMR spectrum indicates that roughly half of the deuterium atoms are located in the MgD_2 phase resonating at 3 ppm, and the remaining deuterium atoms are approximately equally divided over the TiD_y clusters at −43 ppm and in the isolated TiD_z phase at −143 ppm. This yields two additional equations

$$2\nu_{MgD_2}=y\nu_{TiD_y}+z\nu_{TiD_z}, \tag{8}$$

$$y\nu_{TiD_y} = z\nu_{TiD_z}. \quad (9)$$

Finally, from coupled-decoupled deconvolution of the XRD pattern with the same overall restriction $A_{111}:A_{200}=1.4$ (similarly to in the analysis of the pattern of the alloy before deuterium loading), we obtain a peak-area ratio equal to 0.97. Assuming that the left set of reflections consists of the overlapping signals from the isolated TiD_z and the residual Mg phase, and taking the different x-ray scattering factors f_{Ti} and f_{Mg} of Ti and Mg into account, this yields the condition

$$\frac{f_{Mg}^2\nu_{Mg} + f_{Ti}^2\nu_{TiD_z}}{f_{Ti}^2\nu_{Ti}} = 0.97. \quad (10)$$

Here we have assumed that the XRD scattering of the TiD_2 phase is purely controlled by the Ti atoms. Equations (5)–(10) represent six equations for seven unknowns. An upper bound value for the deuterium concentration in the TiD_y clusters y is given by the Knight shift, −43 ppm, which indicates a concentration $y \leq 1.5$.[44] Entering $y=1.5$ we obtain the solution

$$\nu_{Ti} = 0.16,$$

$$\nu_{Mg} = 0.49,$$

$$\nu_{MgD_2} = 0.16,$$

$$\nu_{TiD_z} = 0.08,$$

$$\nu_{TiD_y} = 0.11,$$

$$z = 2.0. \quad (11)$$

Substitution of lower y values yields nonrealistic solutions with D concentrations in the TiD_z phase above 2. The combined quantitative analysis thus suggests a picture of this complex material, in which a quarter of the Mg atoms in the original alloy $Mg_{0.65}Ti_{0.35}$ have been converted into rutile MgH_2 nanodomains, and half of the Ti atoms into either segregated TiD_2, or $TiD_{1.5}$ nanoclusters dispersed between the MgH_2 domains. The formation enthalpy of bulk TiD_2, 144 kJ mol^{-1}, is higher than that of bulk MgH_2, 76 kJ mol^{-1}. The coexistence of MgD_2 and $TiD_{1.5}$ therefore suggests that the latter somehow deviates from the bulk state, perhaps as a result of the small cluster size, or local crystal lattice distortions induced by the surrounding MgD_2.

Scandium and titanium are neighboring elements in the transition-metal series, differing by one $3d$ electron only. From a "chemical" point of view, it is thus remarkable that scandium stabilizes the fluorite structure of magnesium-scandium hydrides, whereas titanium has no such stabilizing effect on hydrides of magnesium-titanium alloys. The different effect is even more amazing, if one considers the fact that *before* hydrogen loading the $Mg_{0.65}Sc_{0.35}$ alloy has a bcc structure, and $Mg_{0.65}Ti_{0.35}$ a (nano)phase separated fcc Mg-rich and fcc Ti-rich structures. With the metal atoms already at the proper fcc positions, one would expect the Mg-rich phase in the $Mg_{0.65}Ti_{0.35}$ alloy to readily transform into the fluorite structure. Instead, however, it is the bcc $Mg_{1-x}Sc_x$ alloy, which transforms into the fluorite structure, whereas the fcc Mg-rich phase in $Mg_{0.65}Ti_{0.35}$ transforms into the rutile structure. A possible explanation for this apparent inconsistency may be an expitaxial rather than chemical mechanism. Comparison of the cell parameters of fcc ScH_2 and fcc TiH_2 with those of rutile and fcc MgH_2 indicates that the cell constants of fcc MgH_2 and ScH_2 match almost perfectly, whereas the cell constant of fcc TiH_2 matches the lattice constant a of rutile MgH_2. By analogy to the coherent coupling in Mg-Ti hydride films,[23] we propose a model for the mixed MgD_2 and TiD_y phases with coupling between the rutile MgD_2 nanodomains and thin layers of fcc TiD_y (Fig. 7).

V. CONCLUSION

After our previous investigation of magnesium-scandium hydride, which has good hydrogen-storage capacity and improved sorption kinetics compared to pure MgH_2, magnesium-titanium deuteride has now been investigated by use of XRD, ND, and MAS ^2H NMR. The material was prepared by exposing ball-milled alloys with overall composition $Mg_{0.65}Ti_{0.35}$ and $Mg_{0.65}Ti_{0.35}Pd_{0.02}$ to deuterium gas at elevated temperature. Before deuterium loading, the alloy consists of a separate fcc Mg and Ti phases with cell parameters 4.42 and 4.28 Å. Even after prolonged deuterium loading at 175 °C the material is only partly deuterated. Deuterium loading causes the formation of a separate fluorite TiD_2 phase, as well as a composite of rutile MgD_2 nanodomains and small clusters or thin layers of $TiD_{1.5}$. Comparison of the cell parameters of fluorite TiD_2 and rutile MgD_2 suggests that the interactions between the rutile MgD_2 and, presumably, fcc TiD_x nanodomains could well be controlled by coherent coupling of the crystal structures. We propose that the different stabilization effect of Sc and Ti on the crystal structure of the corresponding magnesium transition-metal hydrides is directly related to the different lattice constants of the respective fluorite structures of ScH_2 and TiH_2.

ACKNOWLEDGMENTS

The authors are grateful to Brahim Mezari for assistance during the NMR experiments, and to O. Isnard for his help during the ND experiments (CRG-D1B) at the Institut Laue-Langevin in Grenoble. S.S. acknowledges financial support from the Dutch National Research School Combination Catalysis Controlled by Chemical Design (NRSC-Catalysis).

*Corresponding author; p.c.m.m.magusin@tue.nl

[1] A. Seayad and D. M. Antonelli, Adv. Mater. **16**, 765 (2004).
[2] J. L. C. Rowsell and O. M. Yaghi, Angew. Chem., Int. Ed. **44**, 4670 (2005).
[3] B. Sakintuna, F. Lamari-Darkrimb, and Michael Hirscher, Int. J. Hydrogen Energy **32**, 1121 (2007).
[4] I. P. Jain, C. Lal, and A. Jain, Int. J. Hydrogen Energy (to be published).
[5] P. H. L. Notten, M. Ouwerkerk, H. van Hal, D. Beelen, W. Keur, J. Zhou, and H. Feil, J. Power Sources **129**, 45 (2004).
[6] R. A. H. Niessen and P. H. L. Notten, J. Alloys Compd. **404-406**, 457 (2005).
[7] W. P. Kalisvaart, R. A. H. Niessen, and P. H. L. Notten, J. Alloys Compd. **417**, 280 (2006).
[8] M. Latroche, W. P. Kalisvaart, and P. H. L. Notten, J. Solid State Chem. **179**, 3024 (2006).
[9] M. S. Conradi, M. P. Mendenhall, T. M. Ivancic, E. A. Carl, C. D. Browning, P. H. L. Notten, W. P. Kalisvaart, P. C. M. M. Magusin, R. C. Bowman, Jr., S. J. Hwang, and N. L. Adolphi, J. Alloys Compd. **446-447**, 499 (2007).
[10] R. A. H. Niessen and P. H. L. Notten, Electrochem. Solid-State Lett. **8**, A534 (2005).
[11] A. R. Miedema, Physica B **182**, 1 (1992).
[12] T. Mitchell, S. Diplas, P. Tsakiropoulos, J. F. Watts, and J. A. D. Matthew, Philos. Mag. A **82**, 841 (2002).
[13] D. M. Borsa, A. Baldi, M. Pasturel, H. Schreuders, P. Vermeulen, P. H. L. Notten, B. Dam, and R. Griessen, Appl. Phys. Lett. **88**, 241910 (2006).
[14] G. Liang, J. Huot, S. Boily, A. van Neste, and R. Schulz, J. Alloys Compd. **292**, 247 (1999).
[15] G. Liang and R. Schulz, J. Mater. Sci. **38**, 1179 (2003).
[16] R. W. P. Wagemans, J. H. van Lenthe, P. E. de Jongh, A. J. van Dillen, and K. P. de Jong, J. Am. Chem. Soc. **127**, 16675 (2005).
[17] A. Zaluska, L. Zaluski, and J. O. Strom–Olsen, J. Alloys Compd. **288**, 217 (1999).
[18] W. P. Kalisvaart, H. J. Wondergem, F. Bakker, and P. H. L. Notten, J. Mater. Res. **22**, 1640 (2007).
[19] W. P. Kalisvaart and P. H. L. Notten, J. Mater. Res. **23**, 2179 (2008).
[20] P. Vermeulen, H. J. Wondergem, P. C. J. Graat, D. M. Borsa, H. Schreuders, B. Dam, R. Griessen, and P. H. L. Notten, J. Mater. Chem. **18**, 3680 (2008).
[21] P. Vermeulen, P. C. J. Graat, H. J. Wondergem, and P. H. L. Notten, Int. J. Hydrogen Energy **33**, 5646 (2008).
[22] A. Baldi, R. Gremaud, D. M. Borsa, C. P. Baldé, A. M. J. van der Eerdern, G. L. Kruijtzer, P. E. de Jongh, B. Dam, and R. Griessen, Int. J. Hydrogen Energy **34**, 1450 (2009).
[23] D. M. Borsa, R. Gremaud, A. Baldi, H. Schreuders, J. H. Rector, B. Kooi, P. Vermeulen, P. H. L. Notten, B. Dam, and R. Griessen, Phys. Rev. B **75**, 205408 (2007).
[24] D. Kyoi, T. Sato, E. Rönnebro, N. Kitamura, A. Ueda, M. Ito, S. Katsuyama, S. Hara, D. Noréus, and T. Sakai, J. Alloys Compd. **372**, 213 (2004).
[25] E. Rönnebro, D. Kyoi, A. Kitano, Y. Kitano, and T. Sakai, J. Alloys Compd. **404-406**, 68 (2005).
[26] N. L. Adolphi, S. Badola, L. A. Browder, and R. C. Bowman, Phys. Rev. B **65**, 024301 (2001); **69**, 149901(E) (2004).
[27] P. C. M. M. Magusin, W. P. Kalisvaart, P. H. L. Notten, and R. A. van Santen, Chem. Phys. Lett. **456**, 55 (2008).
[28] J. Rodríguez-Carvajal, Physica B **192**, 55 (1993).
[29] J. Jeener, B. H. Meider, P. Bachman, and R. R. Ernst, J. Chem. Phys. **71**, 4546 (1979).
[30] G. A. Morris and R. J. Freeman, J. Magn. Reson. (1969-1992) **29**, 433 (1978).
[31] D. Massiot, F. Fayon, M. Capron, I. King, S. Le Calvé, B. Alonso, J.-O. Durand, B. Bujoli, Z. Gan, and G. Hoatson, Magn. Reson. Chem. **40**, 70 (2002).
[32] See supplementary material at http://link.aps.org/supplemental/10.1103/PhysRevB.81.054107 for supplementary XRD tables, *in situ* neutron-diffraction patterns, thermographic analysis, and static ^{2}H NMR line shapes.
[33] Z. I. Kudabaev, D. R. Torgeson, and A. F. Shevakin, J. Alloys Compd. **231**, 233 (1995).
[34] I. Manna, P. P. Chattopadhyay, P. Nandi, F. Banhart, and H.-J. Fecht, J. Appl. Phys. **93**, 1520 (2003).
[35] C. Suryanarayana and F. H. Froes, J. Mater. Res. **5**, 1880 (1990).
[36] L. Vegard, Z. Phys. **5**, 17 (1921).
[37] P. Vajeeston, P. Ravindran, A. Kjekshus, and H. Fjellvag, Phys. Rev. Lett. **89**, 175506 (2002).
[38] H. G. Schimmel, G. J. Kearley, J. Huot, and F. M. Mulder, J. Alloys Compd. **404-406**, 235 (2005).
[39] H. Koller, G. Engelhardt, A. P. M. Kentgens, and J. Sauer, J. Phys. Chem. **98**, 1544 (1994).
[40] A. P. M. Kentgens, Geoderma **80**, 271 (1997).
[41] M. d'Avezac, N. Marzari, and F. Mauri, Phys. Rev. B **76**, 165122 (2007).
[42] R. C. Bowman, Jr., Hyperfine Interact. **25**, 583 (1985).
[43] M. J. van Setten, S. Er, G. Brocks, R. A. de Groot, and G. A. de Wijs, Phys. Rev. B **79**, 125117 (2009).
[44] R. Goring, R. Lukas, and K. Bohmhammel, J. Phys. C **14**, 5675 (1981).
[45] U. Kaess, G. Majer, M. Stoll, D. T. Peterson, and R. G. Barnes, J. Alloys Compd. **259**, 74 (1997).
[46] U. Stuhr, D. Steinbinder, H. Wipf, and B. Frick, Z. Phys. Chem. **181**, 89 (1993).
[47] B. Stalinski, C. K. Coogan, and H. S. Gurowsky, J. Chem. Phys. **34**, 1191 (1961).
[48] N. L. Adolphi, J. J. Balbach, M. S. Conradi, J. T. Markert, R. M. Cotts, and P. Vajda, Phys. Rev. B **53**, 15054 (1996).
[49] A. Hagemeyer, K. Schmidt-Rohr, and H. W. Spiess, Adv. Magn. Reson. **13**, 85 (1989).
[50] D. E. Favre, D. J. Schaefer, and B. F. Chmelka, J. Magn. Reson. **134**, 261 (1998).
[51] P. C. M. M. Magusin, D. Schuring, E. M. van Oers, J. W. de Haan, and R. A. van Santen, Magn. Reson. Chem. **37**, S108 (1999).
[52] K. B. Efetov and V. N. Prigodin, Phys. Rev. Lett. **70**, 1315 (1993).
[53] D. P. Tunstall, P. P. Edwards, J. Todd, and M. J. Williams, J. Phys.: Condens. Matter **6**, 1791 (1994).
[54] V. E. Zorine, P. C. M. M. Magusin, and R. A. van Santen, J. Phys. Chem. B **108**, 5600 (2004).
[55] B. R. Pauw, W. P. Kalisvaart, S. X. Tao, M. T. M. Koper, A. P. J. Jansen, and P. H. L. Notten, Acta Mater. **56**, 2948 (2008).